

Transitional Modelling of flow over sphere

Sumedh Soman

Department of Mechanical Engineering, K.J.

Somaiya College of Engineering

Abstract

The current study focuses on computing turbulent flow over a spherical body, for different Reynolds number in the transitional flow region, and comparing the obtained data with experimental results. Different mesh configurations were used, and multiple divergence schemes and solver combinations were tested. The results from the simulation runs show that the linear upwind divergence scheme, coupled with Geometric Algebraic Multi Grid (GAMG) solvers, with a careful selection of smoothers show results that match the best with experimental data.

1. Introduction

Transitional turbulence is defined as the process of a flow transitioning from laminar flow to turbulent flow. Transition to turbulence involves several mechanisms, which vary on the basis of the nature of the flow. The present study focuses on modelling flow at transition Reynolds numbers over a sphere. Since the flow for the given scenario could be construed as a parallel flow, the Orr Sommerfeld equation [1], with the help of which it is possible to determine if a perturbation introduced in a parallel, stratified flow will diminish or amplify, can be used to determine whether the flow will transition to turbulence. The equation can be expressed as:

$$(U - c)(\phi_{yy} - k^2\phi) - U_{yy}\phi = \frac{1}{ik Re}[\phi_{yyyy} - 2k^2\phi_{yy} + k^4\phi] \quad (1)$$

This equation cannot be evaluated due to its nonlinear nature. Assuming an inviscid flow enables one to solve the equation. From the solution for inviscid flow, it can be seen that stable solutions can only be calculated for a positive value of c . Furthermore, work by Rayleigh showed that for a parallel inviscid flow, a ‘point of inflexion’ wherein $U_{yy} = 0$ needs to exist for a flow to transition to turbulence. For a Hagen Poiseuille flow case, which is the current flow case being considered, no such inflexion point is present, and therefore the flow remains laminar even at high Reynolds numbers, as long as there is no obstacle, adverse pressure gradient or essentially any ‘trigger’ that can cause a transition to turbulence. The sphere acts as an ‘obstacle’ in this case. As mentioned previously, modelling transitional turbulence has always been difficult due to varied mechanisms that govern transition depending upon the flow, and the large number of nonlocal calculations needed. This feature makes a majority of transitional turbulence models impossible to implement on modern CFD solvers, as they use domain decomposition to compute the solution over several Central Processing Unit (CPU) cores. The LCTM model, also known as

the Gamma-Re-Theta model [3], which is a modified version of the k-Omega SST model cures these difficulties. The given model involves solving two transport equations for intermittency (a non-dimensional quantity designed to predict the onset of turbulence) and for transition momentum thickness Reynolds number ($Re_{\theta t}$). The source terms in these equations depend upon empirical correlations formulated from experimental data. The purpose of the given study is to find the optimum configuration that simulates the flow over a sphere, placed in a flow domain of specified dimensions, at Reynolds numbers in the transition flow regime. C_d (Coefficient of Drag) was plotted as a function of the Reynolds number, and the results were compared with experimental data.

2. Problem Statement

The problem statement was derived from Nakhostin *et al.* [8]. A sphere of dimension D is placed in a domain with dimensions $20D \times 10D \times 10D$, D being the diameter of the sphere. The turbulence length scale was calculated as $0.07 \times D$. The isotropic turbulence ratio was taken as 0.5%.

3. Governing Equations

Two turbulence models were used in the case study, first one being the k-Omega SST model [2] and second being the LCTM Gamma-Re-Theta model [3]. The equations for the k-Omega SST model are as follows:

$$\frac{\partial(\rho k)}{\partial t} + \frac{\partial(\rho u_j k)}{\partial x_j} = P - \beta^* \rho \omega k + \frac{\partial}{\partial x_j} \left[(\mu + \sigma_k \mu_t) \frac{\partial k}{\partial x_j} \right] \quad (2)$$

$$\begin{aligned} & \frac{\partial(\rho \omega)}{\partial t} + \frac{\partial(\rho u_j \omega)}{\partial x_j} \\ &= \frac{\gamma}{\vartheta_t} P - \beta^* \rho \omega^2 + \frac{\partial}{\partial x_j} \left[(\mu + \sigma_\omega \mu_t) \frac{\partial \omega}{\partial x_j} \right] + 2(1 \\ & - F_1) \frac{\rho \sigma_{\omega 2}}{\omega} \frac{\partial k}{\partial x_j} \frac{\partial \omega}{\partial x_j} \end{aligned} \quad (3)$$

(2) Is a transport equation for the turbulent kinetic energy, and (3) is a transport equation for the specific dissipation.

For the LCTM Gamma-Re-Theta model, two additional transport equations for the intermittency and transition momentum Reynolds number need to be solved, along with a modified version of the k-Omega SST model equations, as mentioned in section 1. The equations for intermittency can be expressed as follows:

$$\frac{\partial(\rho\gamma)}{\partial t} + \frac{\partial(\rho u_j \gamma)}{\partial x_j} = P_\gamma - E_\gamma + \frac{\partial}{\partial x_j} \left[\left(\mu + \frac{\mu_t}{\sigma_f} \right) \frac{\partial \gamma}{\partial x_j} \right] \quad (4)$$

$$P_\gamma = F_{length} c_{a1} \rho S [\gamma F_{onset}]^{0.5} (1 - \gamma) \quad (5)$$

The equation for transition momentum thickness Reynolds Number can be expressed as follows: -

$$\frac{\partial(\rho \overline{Re_{\theta t}})}{\partial t} + \frac{\partial(\rho u_j \overline{Re_{\theta t}})}{\partial x_j} = P_{\theta t} + \frac{\partial}{\partial x_j} \left[\sigma_{\theta t} (\mu + \mu_t) \frac{\partial \overline{Re_{\theta t}}}{\partial x_j} \right] \quad (6)$$

$$P_{\theta t} = c_{\theta t} \frac{\rho}{t} (Re_{\theta t} - \overline{Re_{\theta t}}) (1.0 - F_{\theta t}) \quad (7)$$

$$t = \frac{500\mu}{\rho U^2} \quad (8)$$

The equations for turbulent kinetic energy and specific dissipation rate are as follows:

$$\frac{\partial(\rho k)}{\partial t} + \frac{\partial(\rho u_j k)}{\partial x_j} = \tilde{P}_k - \tilde{D}_k + \frac{\partial}{\partial x_j} \left[(\mu + \sigma_k \mu_t) \frac{\partial k}{\partial x_j} \right] \quad (9)$$

$$\frac{\partial(\rho \omega)}{\partial t} + \frac{\partial(\rho u_j \omega)}{\partial x_j} = \frac{\alpha}{\vartheta_t} P_k - D_\omega + C d_\omega + \frac{\partial}{\partial x_j} \left[(\mu + \sigma_\omega \mu_t) \frac{\partial \omega}{\partial x_j} \right] \quad (10)$$

$$\tilde{P}_k = \gamma_{eff} P_k \quad (11)$$

$$\mu_t = \left[\frac{\rho k}{\omega}; \frac{a_1 \rho k}{S F_2} \right] \quad (12)$$

4. Simulation Procedure

4.1 Geometry and Mesh

The snappyHexMesh utility was used to create the mesh for the given study. Two configurations were tested, each with different levels of refinement. The first case had approximately 800,000 cells and the second case had approximately 2,000,000 cells. All configurations had refinements applied near the sphere surface and also in the wake region. The configurations differed only in the number of cells in the mesh overall, as the mesh strategy is identical in both cases. A snapshot of both meshes can be seen below.

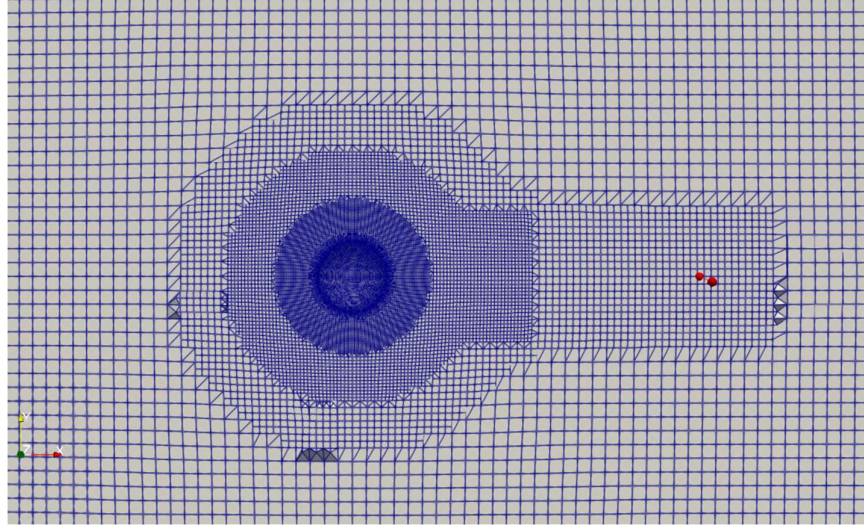


Figure 1: Mesh over the domain (Configuration 1)

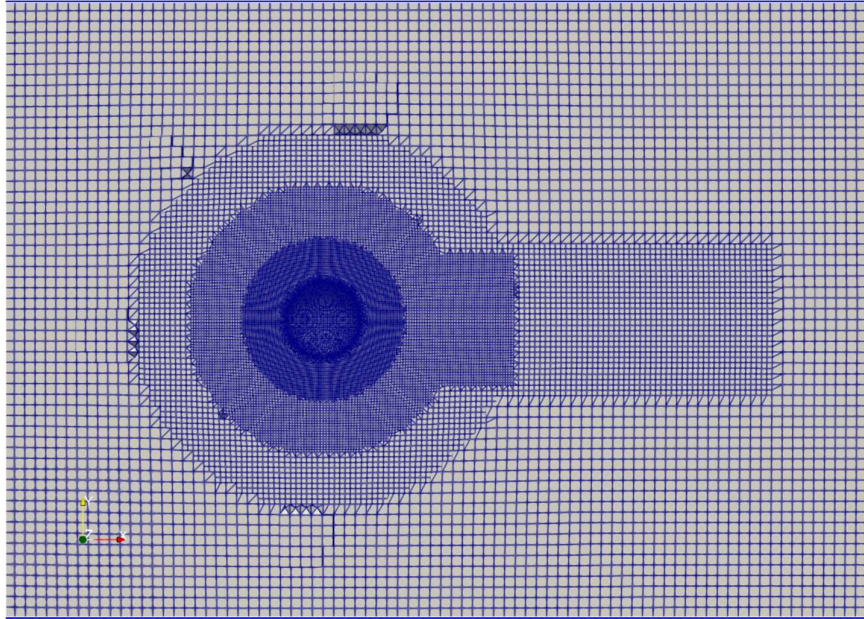


Figure 2: Mesh over the domain (Configuration 2)

4.2 Initial and Boundary Conditions

The mesh was divided into three patches, inlet, outlet and wall. Since the given case is 3D, separate “front” and “back” patches are not required. Since the flow (in the given case) should transition to turbulence only when it encounters the sphere, slip boundary conditions were applied on all the boundaries to ensure that only transport of momentum and energy takes place on the walls of the domain.

The turbulent kinetic energy at the inlet was calculated using the following equation:

$$k_{inlet} = \frac{3}{2}(UI)^2 \quad (13)$$

Where U stands for the velocity and I is the turbulence intensity at the inlet. The specific dissipation rate at the inlet was calculated using the following expression:

$$\omega = \frac{C_\mu^{\frac{3}{4}} k^{\frac{1}{2}}}{l} \quad (14)$$

C_μ is a constant whose value is equal to 0.09, k denotes turbulent kinetic energy, and l is the turbulent length scale.

4.3 Divergence Schemes

Divergence schemes approximate the divergence of a given flux. Gauss Divergence Theorem, which links the surface integrals and volume integrals, is used in the process. Two most commonly used divergence schemes are tested, namely linear Upwind and Upwind. The upwind divergence scheme sets the flux face value equal to the flux value in the upstream direction. For a single dimension, this can be expressed as [4][7]:

$$a_j \phi_j = a_{j-1} \phi_{j-1} + a_{j+1} \phi_{j+1} \quad (15)$$

Where,

$$a_{i-1} = \left(\frac{\Gamma}{dx} \right)_{j-\frac{1}{2}} + \max \left(\rho u_{j-\frac{1}{2}}, 0 \right) \quad (16)$$

$$a_{i+1} = \left(\frac{\Gamma}{dx} \right)_{j+\frac{1}{2}} - \max \left(-\rho u_{j+\frac{1}{2}}, 0 \right) \quad (17)$$

Where Γ is the diffusivity coefficient.

The Linear upwind scheme is a modification of the upwind scheme, which switches between the Mac Cormack scheme and the upwind differencing scheme via a blending operator ϵ which assumes values of either zero or one. The switching operators are only applied when a local eigenvalue test returns a positive value. For a differential equation of the type expressed as-

$$\frac{\partial u}{\partial x} + \frac{\partial F(u)}{\partial t} = 0 \quad (18)$$

The linear Upwind divergence scheme can be expressed as [5]:

$$\begin{aligned} u_j^{i+1} = & 0.5(u_j^{i+1} + u_j^i) - 0.5 \frac{\Delta t}{\Delta x} [\epsilon_j F_j^n - (\epsilon_j - \epsilon_{j-1}) F_{j-1}^n + \epsilon_{j-1} F_{j-2}^n] \\ & - 0.5 \frac{\Delta t}{\Delta x} [-\epsilon_{j-1} F_{j-1}^{n+1} - (\epsilon_j - \epsilon_{j-1} - 1) F_j^{n+1} + (1 - \epsilon_{j-1}) F_{j+1}^{n+1}] \end{aligned} \quad (19)$$

where,

$$(\epsilon_j, \epsilon_{j-1}) = \begin{cases} (0,0) & \text{MacCormack scheme} \\ (0,1) & \text{MU transition operator} \\ (1,0) & \text{UM transition operator} \\ (1,1) & \text{Upwind scheme} \end{cases} \quad (20)$$

4.4 Pressure-Velocity coupling algorithms and solvers

Several solver and Pressure-Velocity configurations were tested. The SIMPLE algorithm was decided as the optimal Pressure Velocity coupling algorithm, due to its blend of lower computational cost and high accuracy for aerodynamic flows simulated using RANS models, as shown by Robertson *et al.* [6]. Extensive tests were carried out with regards to solver and smoother selection. Based on the author's previous tests on the flow over a flat plate case (ERCOFTAC T3A) GAMG (Geometric Algebraic Multi Grid) solvers were chosen for all the variables to be solved. Smoother selection was done on the basis of the nature of the global matrix to be solved. For asymmetric matrices, the DICGaussSeidel smoother was found to give the best results. For symmetric matrices, the DILUGaussSeidel solver was chosen, and was found to have the highest rate of convergence. The model was run for different Reynolds numbers, ranging from 1×10^5 to 5×10^5 . The model was run for 10,000 iterations for every single Reynolds number, and the C_d value was averaged over iterations.

4.5 Comparison between various divergence schemes

Figure 3 shows the C_d value as a function of Reynolds number for different divergence schemes, using the first mesh configuration. It can be clearly observed that the linear upwind scheme is producing the results that match the best with experimental values. The simulation setup with upwind divergence scheme displayed numerical instabilities after 2×10^5 Reynolds number. This validates the claim made by Robertson *et al.* [6] regarding the suitability of the linear upwind divergence scheme. Linear Upwind is eminently suitable for the given case due to the second order nature of the constituent schemes as well as its ability to switch between the Mac Cormack and Upwind divergence scheme, enabling accurate simulation of flow around discontinuities.

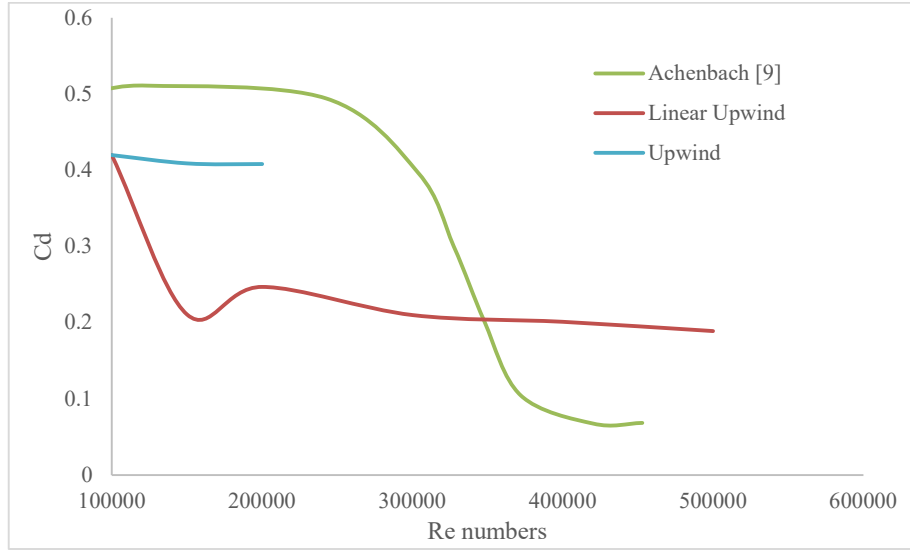


Figure 3: C_d expressed as a function of Reynolds numbers, for different divergence schemes

4.6 Comparison between Mesh Configurations

Figure 4 shows the C_d value as a function of Reynolds number for different mesh configurations, specifically, one mesh configuration with 25 refinement layers applied on the surface of the sphere, with a total cell count approaching 1M cells, and another configuration with 25 refinement layers applied on the surface of the sphere and total cell count exceeding 2M cells. It can be observed that the configuration with lesser cells is predicting a higher C_d in the post-critical region, as compared to experimental values, while the configuration with 2M cells is predicting values that are closer to experimental results. In both the cases, the trend of the computational results is differing from experimental values, as the C_d values begin to fall after 3×10^5 Reynolds number whereas in the computational results, the same ‘fall’ is observed around 1×10^5 Reynolds number itself.

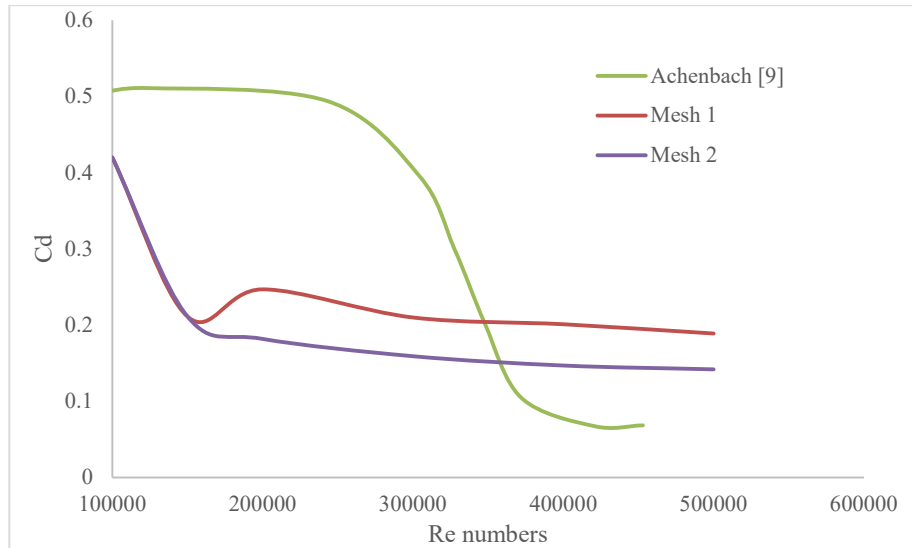


Figure 4: C_d expressed as a function of Reynolds numbers, for different meshing schemes

4.7 Comparison between k-Omega SST and Gamma-Re-Theta

Figure 5 shows the C_d value as a function of Reynolds number for k-Omega SST and Gamma-Re-Theta turbulence model configurations. It can be seen that the trend of the k-Omega SST plot does not match with the experimental predictions, and deviates even further as compared to the Gamma-Re-Theta plot. The k-Omega SST model doesn't include any special provisions to capture transition effects appropriately, and hence this deviation is observed. Also, the wake regions (as shown in Figure 6) predicted by both models are noticeably different, with the gamma-Re-Theta model's predicted wake region being noticeably larger than the wake region predicted by k-Omega SST, as k-Omega SST cannot capture the transition process.

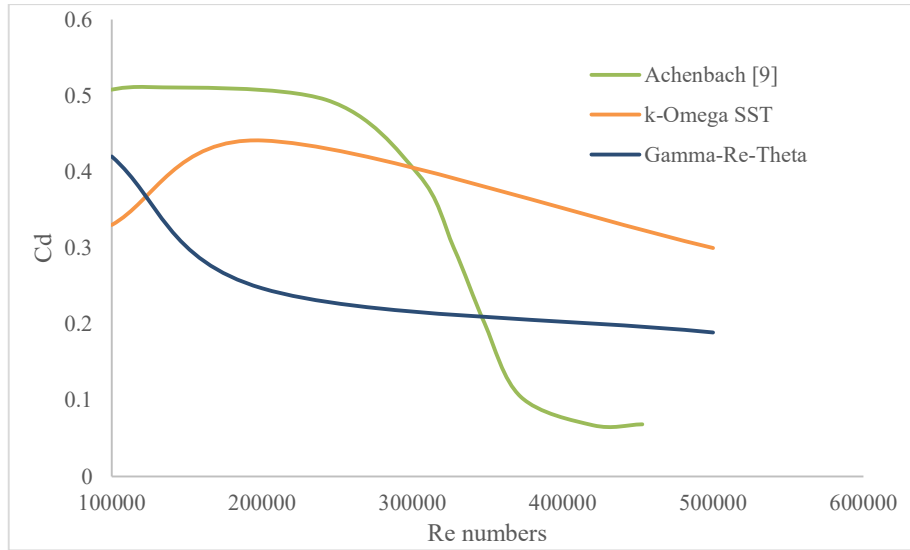


Figure 5: C_d expressed as a function of Reynolds numbers, for different divergence schemes

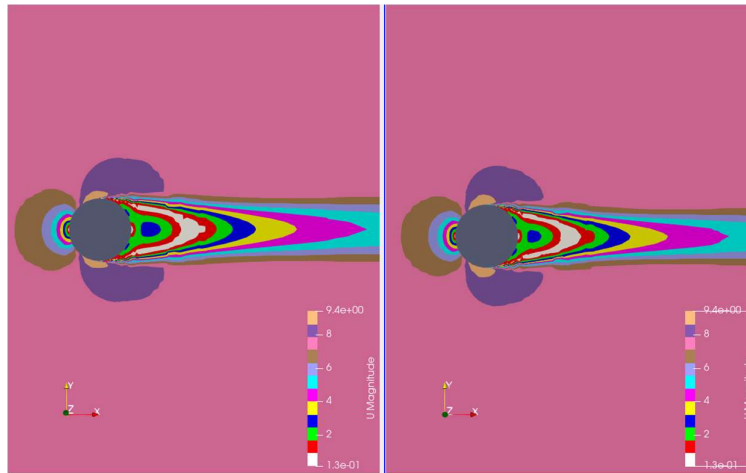


Figure 6: Wake region predictions for two different turbulence models. The k-Omega SST wake prediction is shown on the right, while the Gamma-Re-Theta model prediction is shown on the left.

References

- [1] Kundu, Pijush P.; Cohen, M.; Dowling, R.; Chapter 11 - Instability, Editor(s): Pijush K. Kundu, Ira M. Cohen, David R. Dowling, Fluid Mechanics (Sixth Edition), Academic Press, 2016, Pages 533-602, ISBN 9780124059351, <https://doi.org/10.1016/B978-0-12-405935-1.00011-3>.
- [2] Menter, F. R. (1992). Improved two-equation k-omega turbulence models for aerodynamic flows. *Nasa Sti/recon Technical Report N*, 93, 22809
- [3] Menter, F.R., Langtry, R. & Völker, S. Transition Modelling for General Purpose CFD Codes. *Flow Turbulence Combust* **77**, 277–303 (2006). <https://doi.org/10.1007/s10494-006-9047-1>
- [4] Spalding, D. B. (1972). A novel finite difference formulation for differential expressions involving both first and second derivatives. *International Journal for Numerical Methods in Engineering*, 4(4), 551-559.
- [5] Warming, R. F., & Beam, R. M. (1976). Upwind second-order difference schemes and applications in aerodynamic flows. *AIAA Journal*, 14(9), 1241-1249.
- [6] Robertson, E., Choudhury, V., Bhushan, S., & Walters, D. K. (2015). Validation of OpenFOAM numerical methods and turbulence models for incompressible bluff body flows. *Computers & Fluids*, 123, 122-145.
- [7] Versteeg, H. K., & Malalasekera, W. (2007). *An introduction to computational fluid dynamics: The finite volume method*. Harlow, England: Pearson Education Ltd.
- [8] Nakhostin, S. M., & Giljarhus, K. E. T. (2019, November). Investigation of transitional turbulence models for CFD simulation of the drag crisis for flow over a sphere. In *IOP Conference Series: Materials Science and Engineering* (Vol. 700, No. 1, p. 012007). IOP Publishing.
- [9] Achenbach, E. (1972). Experiments on the flow past spheres at very high Reynolds numbers. *Journal of fluid mechanics*, 54(3), 565-575.